Rock Mech Rock Eng (2010) 43:3–19
DOI 10.1007/s00603-009-0027-3

ORIGINAL PAPER

An Integrated Numerical Modelling–Discrete Fracture Network Approach Applied to the Characterisation of Rock Mass Strength of Naturally Fractured Pillars

Davide Elmo · Doug Stead

Received: 24 April 2008 / Accepted: 28 November 2008 / Published online: 23 January 2009
© Springer-Verlag 2009

Abstract Naturally fractured mine pillars provide an excellent example of the importance of accurately determining rock mass strength. Failure in slender pillars is predominantly controlled by naturally occurring discontinuities, their influence diminishing with increasing pillar width, with wider pillars failing through a combination of brittle and shearing processes. To accurately simulate this behaviour by numerical modelling, the current analysis incorporates a more realistic representation of the mechanical behaviour of discrete fracture systems. This involves realistic simulation and representation of fracture networks, either as individual entities or as a collective system of fracture sets, or a combination of both. By using an integrated finite element/discrete element–discrete fracture network approach it is possible to study the failure of rock masses in tension and compression, along both existing pre-existing fractures and through intact rock bridges, and incorporating complex kinematic mechanisms. The proposed modelling approach fully captures the anisotropic and inhomogeneous effects of natural jointing and is considered to be more realistic than methods relying solely on continuum or discontinuum representation. The paper concludes with a discussion on the development of synthetic rock mass properties, with the intention of providing a more robust link between rock mass strength and rock mass classification systems.

D. Elmo (✉)
Golder Associates Ltd, Greater Vancouver Office,
Burnaby, BC, Canada
e-mail: Davide_Elmo@golder.com

D. Stead
Department of Earth Sciences,
Simon Fraser University, Burnaby, BC, Canada

Keywords Numerical modelling · Rock pillars · Rock mass properties · Rock mass characterisation · Discrete fracture network

1 Introduction

Rock pillars can be defined as the in situ rock between two or more underground openings. In the design of room-and-pillar or stope-and-pillar systems, the loading capacity of a pillar, i.e. its strength, is equally as important as the stability of the roof and walls (Nordlund et al. 1995). Studies on hard rock pillars date back to the 1970s and 1980s. Important recent contributions to the subject include those of Martin and Maybee (2000), Diederichs et al. (2002), Fang and Harrison (2002) and Roberts et al. (2007). Figure 1 illustrates typical failure mechanism of a naturally fractured pillar, including (a) failure by lateral kinematic release of preformed blocks due to the increasing vertical load, (b) failure as a result of the formation of inclined shear fractures transecting the pillar, typically in relative low width-to-height (W:H) ratio pillars and (c) failure along a set of transgressive fractures occurring if the angle of inclination of the fractures to the pillar principal axis of loading exceeds their angle of friction. Overall, the mechanical response of a pillar is directly linked to the presence of geological structures and it can be safely assumed that these effects would be more noticeable for slender pillars.

The most generally accepted techniques for estimating pillar strength (defined as the ultimate load per unit area of a pillar) use empirical formulae based on survey data from actual mining conditions (Martin and Maybee 2000). However, empirical methods do not consider specific failure mechanisms and their limitations are associated with

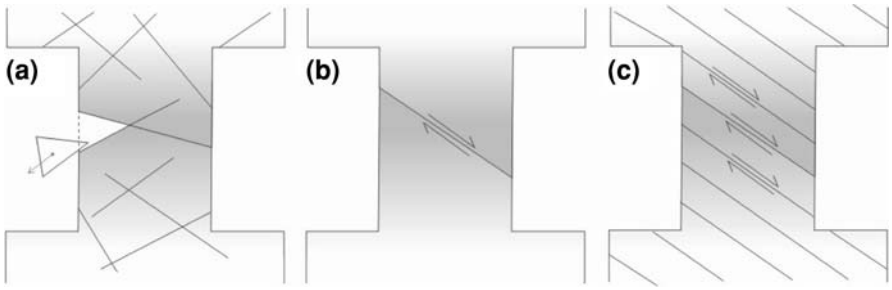

Fig. 1 Typical failure mechanism of a naturally fractured pillar (after Nordlund et al. 1995): **a** occurrence of preformed blocks, **b** formation of inclined shear fractures transecting the pillar and **c** transgressive fractures

their intrinsic derivation from specific material properties (observed size, shape and stress conditions). Numerical methods overcome some of the limits of the empirical methods and provide an opportunity to increase our fundamental understanding of the factors governing the strength and deformational response of jointed rock masses. Continuum and discontinuum models can be utilised to simulate multifracturing phenomena and the mechanical behaviour of discrete systems. However, neither approach alone can capture the interaction of existing discontinuities and the creation of new fractures through fracturing of the intact rock material (Coggan and Stead 2005). Hybrid models have been increasingly used in rock engineering, combining the above methods in order to eliminate undesirable characteristics while retaining as many advantages as possible. This is illustrated by Elmo (2006) and Pine et al. (2006) who recently introduced a new numerical modelling approach for naturally fractured rock masses that combines the representation of existing rock jointing with the use of a loading model which fully accounts for the style of jointing. The current paper reviews the main characteristics of the aforementioned approach and presents recent results with specific emphasis on the characterisation of rock mass strength for naturally fractured hard-rock pillars. Significant contributions of this paper include a better characterisation of the anisotropic and inhomogeneous effects of natural jointing and a discussion on the development of so-called synthetic rock mass properties.

2 A DFN Approach as a Tool to Simulate More Realistic Geological Models

Rock discontinuities can be characterised in terms of their orientation, intensity and spatial distribution, in addition to their strength and deformability. With the exception of fully explicit modelling of an individual fracture or simplified fracture sets, the use of a stochastic discrete fracture network (DFN) approach provides the best option for creating realistic geometric models of fracturing, reflecting the heterogeneous nature of a specific fractured rock mass. The basis of DFN modelling is the characterisation of each discontinuity set within a structural domain using statistical distributions to describe variables such as orientation, persistence and spatial location of the discontinuities. The DFN approach maximises the use of discontinuity data from mapping of exposed surfaces, boreholes and or other sources of spatial information (e.g. digital photogrammetry and LiDAR).

The proprietary code FracMan (Dershowitz et al. 1998; Golder Associates 2007) is the platform used in the current paper for DFN data synthesis. The typical process involved in the generation of a DFN model for geomechanics analysis is described in Elmo (2006) and Pine et al. (2006). By coupling a DFN model with a geomechanics analysis, the same authors have demonstrated that it is possible to take full advantage of the use of accessible data, notably the intact rock properties and the orientation, persistence and intensity of discontinuities, whilst also explicitly accounting for size and shape (scale) effects (Fig. 2).

3 Geomechanics Analysis: The Hybrid FEM/DEM Code ELFEN

The hybrid FEM/DEM approach combines aspects of both finite elements and discrete elements with fracture mechanics principles. The finite-element-based analysis of continua is merged with discrete-element-based transient dynamics, contact detection and contact interaction solutions (Munjiza 2004). The use of fracture mechanics principles allows the realistic simulation of brittle-fracture-driven processes and a full consideration of the failure kinematics. The code ELFEN (Rockfield 2007) is a 2D/3D numerical modelling package incorporating hybrid FEM/DEM techniques with fracture capability that has recently found increasing use in rock mechanics. Detailed descriptions of the constitutive material models and fracture mechanics criteria implemented in ELFEN can be found in Klerck (2000), Owen et al. (2004) and Pine et al. (2007).

Cai and Kaiser (2004) have illustrated the application of ELFEN in the numerical simulation of indirect tensile (Brazilian) testing. Stead et al. (2004) and Eberhardt et al. (2004) applied ELFEN to rock slope failure analysis. Elmo et al. (2005), Pine et al. (2006) and Elmo (2006) used the ELFEN code in the study of mine pillars. Yan et al. (2007)

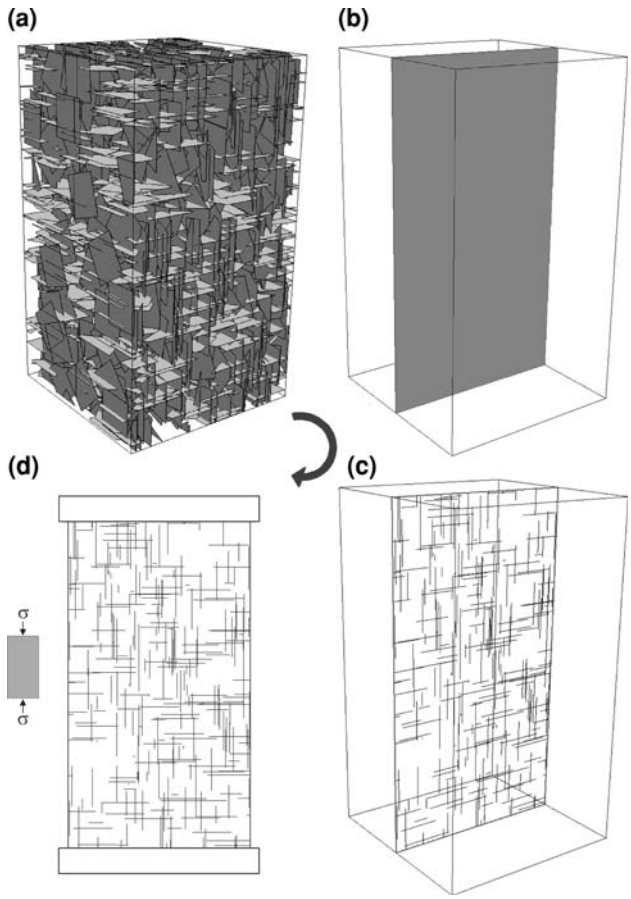

Fig. 2 Example of the coupling of a DFN model with a geomechanics analysis. **a** 3D DFN model, **b** section plane, **c** fracture traces on section plane and **d** fracture traces transferred to the geomechanics model (2D uniaxial case is represented)

and Stefanizzi (2007) used the code ELFEN to simulate step-path failure mechanisms and to characterise the mechanical behaviour of layered rocks, respectively. Karami and Stead (2008) described the use of ELFEN in the simulation of shear box tests and the effects of varying joint roughness profiles. The use of an integrated FEM/DEM-DFN approach to characterise subsidence associated with block cave mining and surface to underground interaction have recently been discussed by Vyazmensky et al. (2008) and Elmo et al. (2008).

4 Initial Geomechanics Modelling and Characterisation of Pillar Strength

4.1 Characterisation of the Anisotropic Strength of Naturally Jointed Pillars

In hard-rock and low-stress environments existing fractures control the potential failure modes and the associated extent of failure. This is particularly true for mine pillars, whose loading capacity may well be drastically reduced by the occurrence of natural fracture planes providing less resistance to sliding.

This initial section of the paper presents a study on progressive pillar failure assuming a series of conceptual 2D 4 m × 8 m pillar models containing a predefined fracture geometry generated using the code FracMan. The basic DFN model includes two orthogonal joint sets dipping at 0°–90°, with the fracture radius distribution defined according to a lognormal function, with descriptive parameters of 0.25 m (mean) and 0.25 m (SD). Models with different fracture radius and fracture orientation are obtained, respectively, by increasing the initial fracture radius according to a specified length multiplier and by rotating the fractures counterclockwise. Subsequently, the fracture geometry data from the 3D FracMan realisations are transferred to the code ELFEN, considering a 2D section as illustrated in Fig. 3. In total 21 different fracture geometries have been investigated in the current analysis, by combining three fracture length (on the 2D section) and seven orientation models (Table 1). The modelled pillars are loaded as if they were subjected to uniaxial laboratory loading conditions and the prefractured rock throughout the full height of the rock pillar is modelled using a coupled Rankine/Mohr–Coulomb fracturing criterion. Table 2 lists the modelling properties of both the intact rock and the rock fractures. Rock cohesion and friction were determined using the program RocLab (Rocscience 2007; Hoek et al. 2002) assuming a value for σ_{ci} of 100 MPa and Hoek–Brown parameters of $s = 1$ and $m_i = 12$ (dolomite), over a limited range of confining stress. The tensile strength was estimated as one-tenth of the assumed uniaxial compressive strength.

Figure 4 shows the simulated axial stress–strain response for the model with fracture mean length of 0.93 m and 0°–90° jointing. For the modelled pillar, the fracture evolution at several stages of loading is compared with the classification of pillar conditions by Roberts et al. (1998). The initial fractures (from the DFN model) extend very little until stage I. By stage II, new fracturing occurs in the core and subsequently stress redistribution controlled by jointing contributes to the left side of the pillar becoming partially detached (stage III). By stage IV a load-bearing core is established with further blocks becoming detached. Past the peak (stage V), the pillar core is almost wholly consumed by fracturing.

Figures 5, 6 and 7 show the modes of failure for selected pillar models, whilst the corresponding stress–strain curves are included in Fig. 8. The modelling results clearly capture the anisotropic response in strength and deformability, as a function of fracture length and fracture inclination with respect to the pillar vertical axis. The modelled curves (Fig. 9) show comparable trends to experimental data (e.g. Hoek and Brown 1980; Brady and Brown 1993).

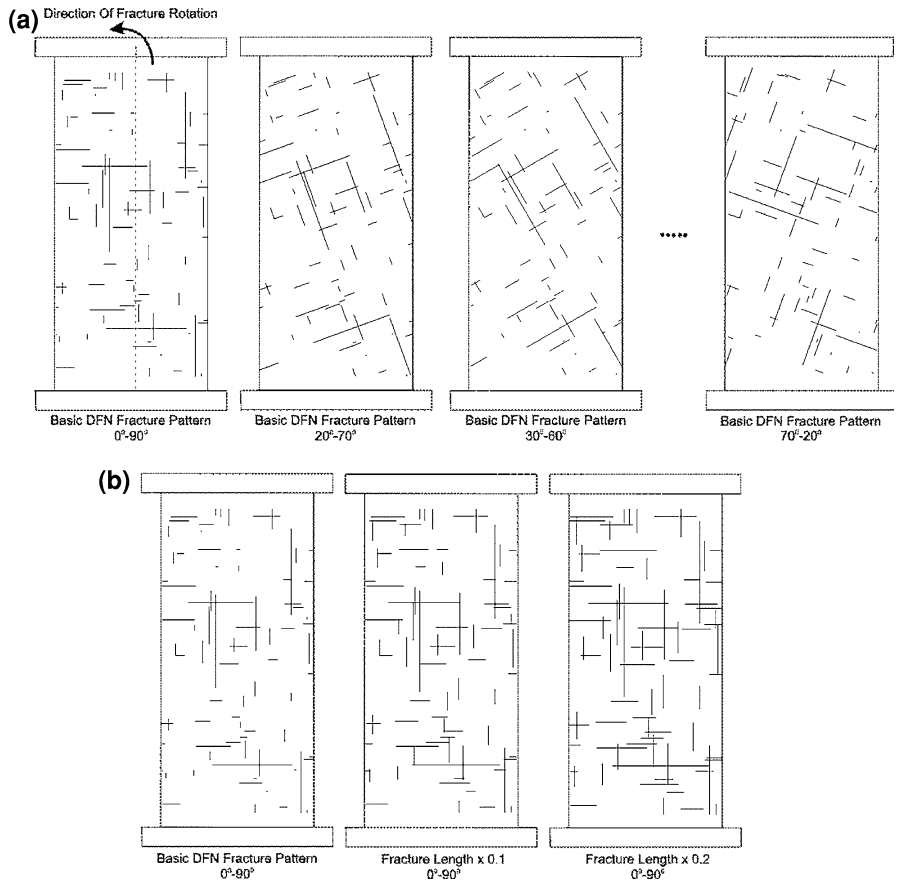

Fig. 3 Two-dimensional geomechanics conceptual modelling. **a** Basic DFN model showing direction of fracture rotation and **b** basic DFN model with indication of the multiplying factor used in FracMan to vary fracture length

Table 1 Geometrical characteristics of the different modelling scenarios

Mean length of fractures (m)	Inclination of predefined fracture network (Set 1°–Set 2°)						
0.43	0–90	20–70	30–60	40–50	50–40	60–30	70–20
0.73	0–90	20–70	30–60	40–50	50–40	60–30	70–20
0.93	0–90	20–70	30–60	40–50	50–40	60–30	70–20

Table 2 Assumed material properties used in the analysis for characterisation of the anisotropic strength of naturally jointed pillars

Property (rock mass)	Unit	Value	Property (joints)	Unit	Value
Tensile strength, σ_t	MPa	10	Fracture cohesion, c_f	MPa	0
Fracture energy, G_f	J m^{-2}	63	Fracture friction, ϕ_f	°	35
Young's modulus E	MPa	60,000	Normal penalty, P_n	GPa m^{-1}	5
Poisson's ratio, ν		0.25	Tangential penalty, P_t	GPa m^{-1}	0.5
Internal cohesion, c_i	MPa	20			
Internal friction, ϕ_i	°	45			

Percentages of strength variation with fracture length and joint inclination for the models in Fig. 8 are listed in Table 3. The analysis has shown that, due to the more critical jointing inclination, the response of the models with 50°–40° joint sets is least affected by the increased fracture length. The combined effect of longer and steeply dipping fractures (Figs. 7 and 8; model 50°–40°) is such that the pillar fails at a much lower strength (26% of the corresponding model with 0°–90° joints), and mainly by blocks sliding and rotating along the fracture planes dipping at 50°. For the models with 0°–90° joint inclination the amount of fracturing through the intact rock mass decreases and plastic deformation increases, respectively, with increasing fracture length. The actual fracture pattern (and

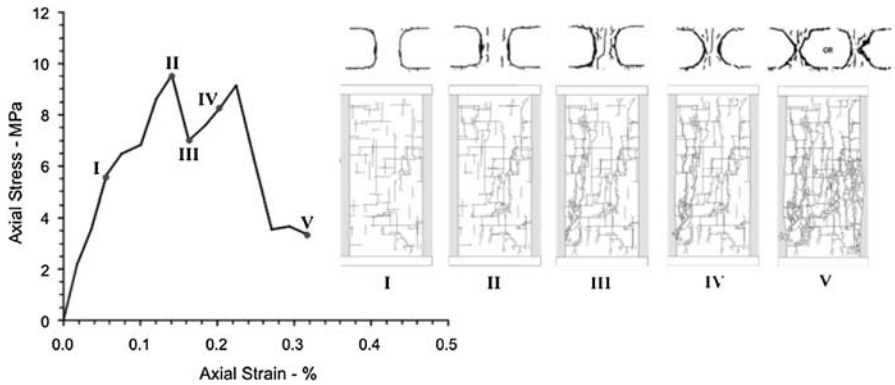

Fig. 4 Simulated axial stress–strain response for the model with fracture mean length of 0.93 m and 0°–90° jointing. Also indicated is the fracturing evolution at different stages of the simulation (I–V) and the assumed correlation with the visual classification of pillar conditions by Roberts et al. (1998)

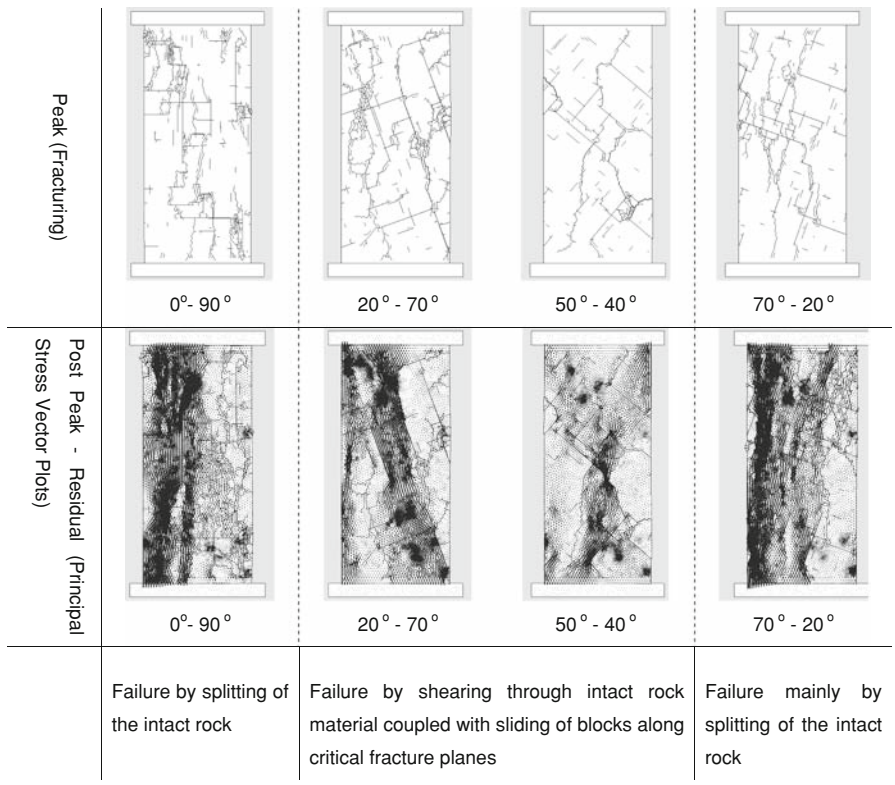

Fig. 5 Modes of failure for selected simulated pillars with 0.43 m mean fracture length

associated degree of asymmetry) is the key parameter controlling the modes of failure of the simulated pillars, resulting in a combination of more than one mechanism. The most dominant modes of failure include: (a) splitting of the intact rock, (b) shearing through intact rock material and (c) composite rotation–sliding of blocks along critical fractures. Splitting occurs as a result of tensile stresses developing within the simulated pillars, with newly formed cracks being generated parallel to the major principal stress direction (Fig. 10a). For a an initial DFN geometry consisting of sub-horizontal/sub-vertical joints, the failure response of the simulated pillars is characterised by the development of shearing planes, extending through the intact material and the pre-existing joints. For a combination of relative steeply dipping joint sets (50°–40°), block rotation and sliding are observed, the portion of rock in between the predefined joints remaining almost intact (Fig. 10b). This mode of failure is typically associated with relatively large deformations in a direction normal to the major principal stress direction. The simulations have shown that the stress distribution across the pillars changes greatly from its initial state as a consequence of the applied loading and is largely controlled by the initial jointing conditions. This is demonstrated by observing the maximum/minimum principal stress vector plots in Figs. 5, 6 and 7. Principal stress vectors are plotted for every node in the finite element mesh and the stresses are shown as two perpendicular lines, which indicate their directions and magnitudes (the darker tone corresponding to the major principal stress). In the post-peak region, as the outer layers

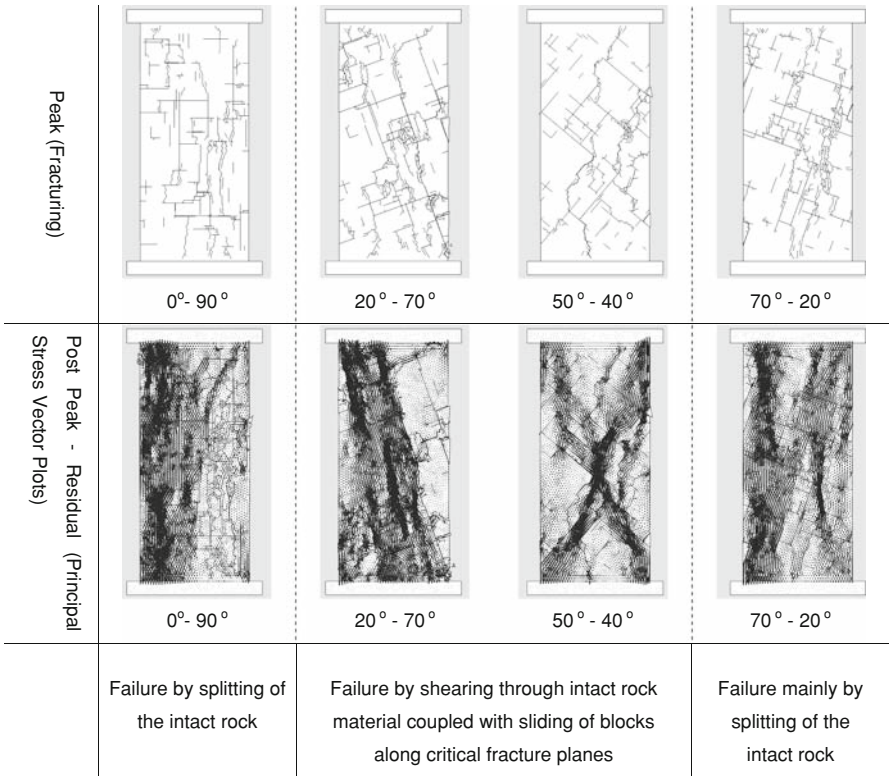

Fig. 6 Modes of failure for selected simulated pillars with 0.73 m mean fracture length

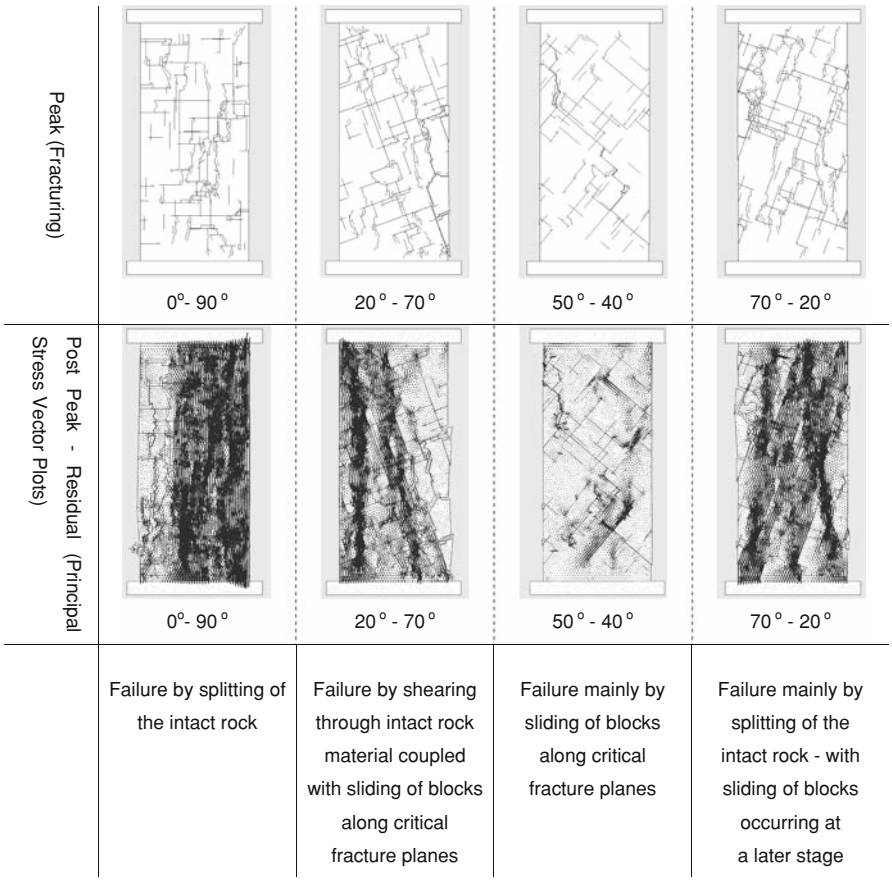

Fig. 7 Modes of failure for selected simulated pillars with 0.93 m mean fracture length

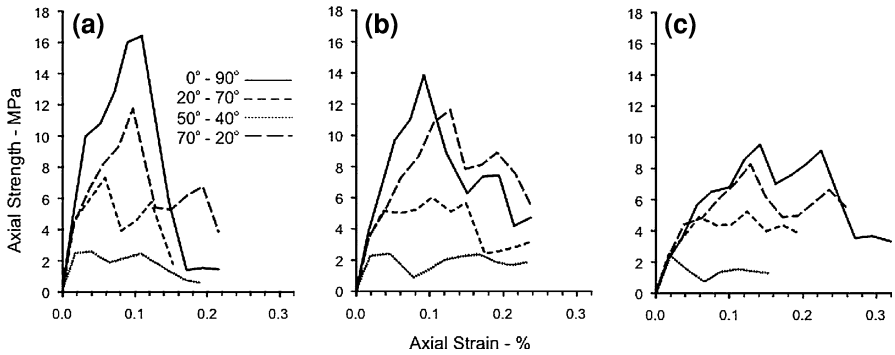

Fig. 8 Simulated axial stress–strain response for the modelled jointed pillars with mean fracture length of **a** 0.43 m, **b** 0.73 m and **c** 0.93 m, respectively

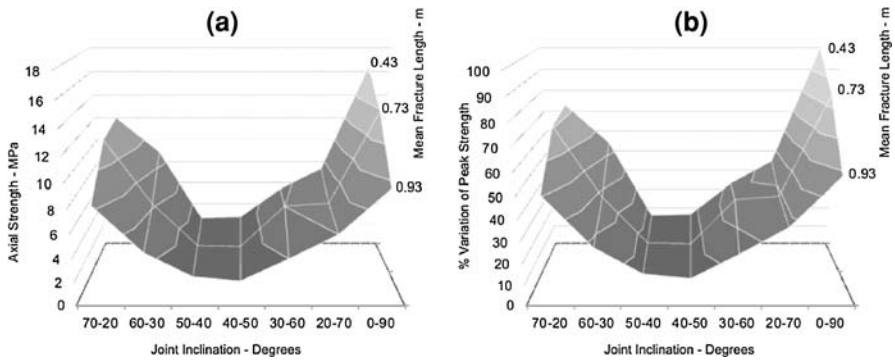

Fig. 9 Variation of axial strength as a function of fracture inclination and length. Absolute values (**a**) and relative variation as a percentage of the 0°–90° model with 0.43 m mean fracture length (**b**)

Table 3 Percentages of strength variation with fracture length and joint inclination for the models in Fig. 8

Mean length of fractures (m) on 2D section	Inclination of predefined fracture network (Set 1°–Set 2°)			
	0–90	20–70	50–40	70-20
Variation of peak strength (%) with length (fixed joint inclination)				
0.43	100	100	100	100
0.73	84	85	94	97
0.93	58	82	96	69
Variation of peak strength (%) with joint inclination (fixed length)				
0.43	100	45	16	73
0.73	100	45	18	84
0.93	100	56	26	86

of rock become detached and the pillar eventually yields, the stress directions clearly appear to be concentrated in the relatively more intact portion of the pillar, reflecting the asymmetry of the failure process.

4.2 Analysis of Scale Effects

The uncertainty in predicting the behaviour of a fractured mass under uniaxial stress is clearly associated with scale effects (Singh et al. 2002). Excluding the cases of either a very closely fractured or an almost massive rock mass, the mechanical response is nonuniform and is affected by the orientation, spacing and persistence of the discontinuities (Pine and Harrison 2003). In the current study, a FracMan-generated fracture pattern has been used to investigate the variation of simulated pillar strength with pillar size for a constant pillar width-to-height (W:H) ratio. It is noted that the FracMan DFN model has been developed based on mapped data from an actual but unnamed room-and-pillar mine. The size of the modelled pillars has been progressively reduced by considering smaller sections of an initial larger pillar model, keeping the W:H ratio constant at 0.5. The geometrical definition of the model is illustrated in Fig. 11, whilst Table 4 lists the properties of the intact rock and rock. Figure 12 shows the variation of the simulated pillar strength as a function of pillar width. Smaller pillar models are characterised by a relatively higher strength, with failure primarily occurring by fracturing through intact rock. For the modelled pillars the variation in strength, expressed as a percentage of model D, is 63%,

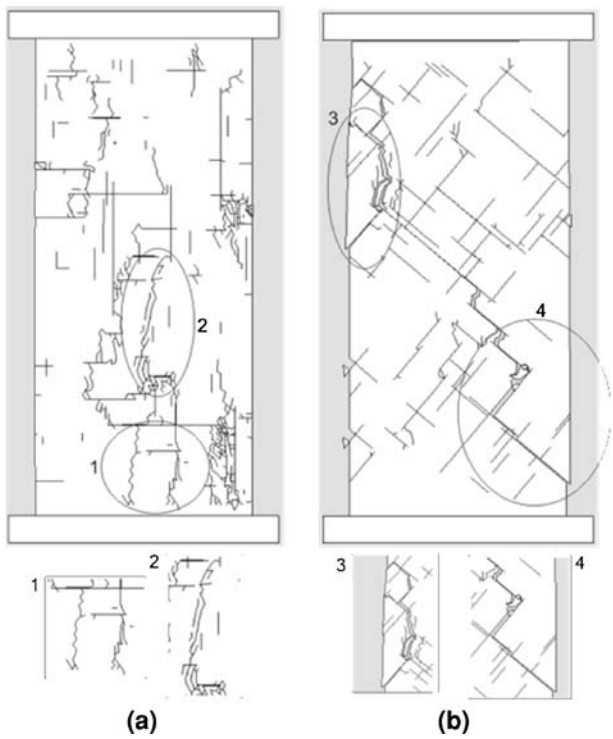

Fig. 10 Typical failure mechanisms of the simulated pillars. **a** Tensile splitting (model 0°–90°, mean fracture length 0.43 m) and **b** composite rotation–sliding of blocks along critical fractures (model 50°–40°, mean fracture length 0.93 m), respectively

26% and 18% for models C, B and A, respectively. For increasing pillar width (W:H ratio of 0.5), the strength of the simulated pillars appears to become independent of the actual pillar dimensions. The results qualitatively agree with the theoretical reduction in mass strength for increasing size observed for an intact rock specimen (Hoek and Brown 1980), which is given according to:

$$\sigma_C = \sigma_{C50}\left(\frac{50}{d}\right)^{0.18}, \quad (1)$$

where d is the diameter of the rock sample and σ_{C50} is the uniaxial strength of a 50-mm-diameter intact rock specimen. It is safe to assume that a progressive reduction in the pillar width will result in the structural character of the modelled pillars approaching intact rock mass conditions (i.e. fewer to no pre-inserted fractures will be contained within the pillar model). It is expected that the shape of the modelled curve will change according to varying jointing conditions, assuming that no fracture is much more persistent or has much weaker properties than the other fractures in the network.

Variation in width also has a clear impact on the deformational behaviour of the modelled pillars. In particular, pillars of smaller width, for which the failure process is dominated by new stress-induced fracturing, appear to behave in a more brittle manner compared with pillars of larger width. For relatively wider pillars the observed ductile response can be associated with both an increasing confining effect, as the pillar width is enlarged, and the inclusion in the rock mass of a larger number of discontinuities. Figure 13a and b, respectively, show the simulated axial stress–axial strain response and the associated variation of deformation modulus (E_m) with axial strain. The initial reduction of E_m observed at approximately 0.04% axial strain for models B and C (Fig. 13b) corresponds to a process of extension and coalescence of new fractures (Fig. 13c). The difference between maximum and minimum deformation modulus (max–min E_m, normalised to model D), as deformation progresses, is shown in Fig. 13d. The data clearly shows a general decreasing trend with increasing pillar width. A value of unity is assumed to represent elasto-brittle conditions (model D), whilst a difference of zero would imply complete elasto-plastic behaviour.

The results provide an example of the definition of both a representative elementary volume (REV) for a rock mass and reduction of its unit mass strength/deformability with increasing volume up to a REV. For a given fractured rock mass, it is possible to define a minimum volume of rock (area for the 2D case) having representative values of rock mass properties. The analysis suggests that the brittle-

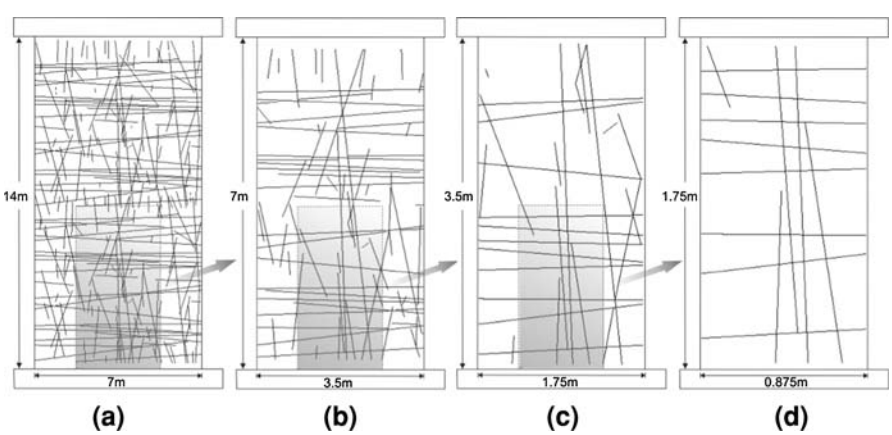

Fig. 11 Geometrical definition of the pillar models investigating the importance of scale effects

Table 4 Assumed material properties for analysis of scale effects

Property (rock mass)	Unit	Value	Property (joints)	Unit	Value
Tensile strength, σ_t	MPa	12	Fracture cohesion, c_f	MPa	0.25
Fracture energy, G_f	J m^{-2}	63	Fracture friction, ϕ_f	°	45
Young's modulus E	MPa	84,000	Normal penalty, P_n	GPa m^{-1}	200
Poisson's ratio, ν		0.25	Tangential penalty, P_t	GPa m^{-1}	20
Internal cohesion, c_i	MPa	20			
Internal friction, ϕ_i	°	45			

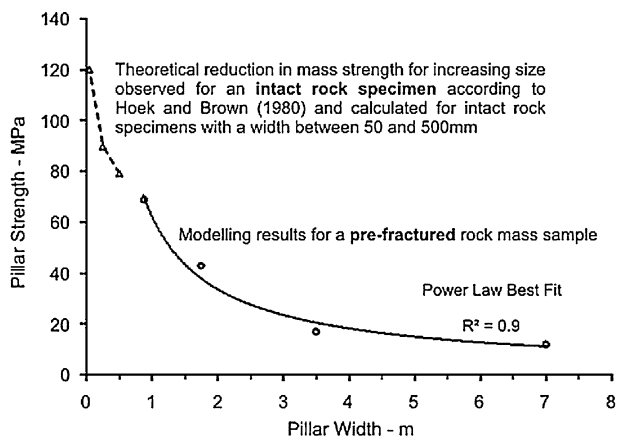

Fig. 12 Analysis of scale effects for the pillar models A–D indicated in Fig. 11. Variation of the simulated pillar strength as a function of pillar width (assumed W:H equal to 0.5)

to-plastic transition, expressed in terms of max–min E_m, has fully occurred as the rock mass has reached the REV. The representative volume is ultimately a function of fracture length and should be large enough to include sufficient fracture intersections. As discussed in Sect. 6, this latter remark has major implications with respect to the characterisation of rock mass strength and the definition of synthetic rock mass properties.

5 Characterisation of Rock Mass Strength: The Middleton Mine Case Study

Initial applications and trial runs for the proposed geomechanics approach have been presented in Pine et al. (2006) and Elmo (2006). Using the same case study, the authors extend this work and present the results of a more detailed and comprehensive program of analyses. Middleton mine (Derbyshire, UK) is a classic square room-and-pillar mining operation (Fig. 14) with drift access working mostly under a cover of about 100 m. The excavation is within the payable Hoptonwood limestone. This is a massive cream-grey, coarse-medium grained carboniferous limestone, approximately 80 m thick and interbedded with clay

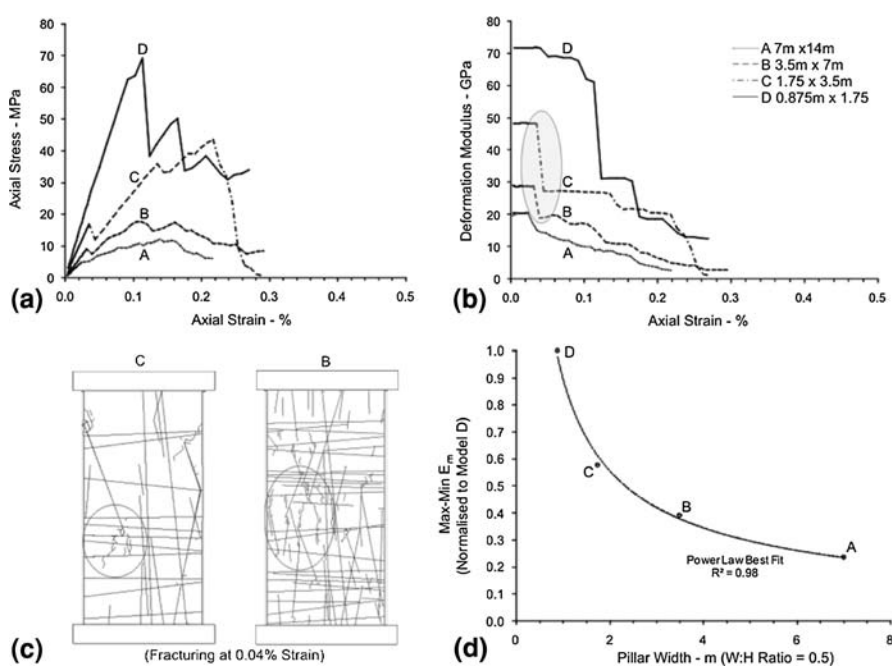

Fig. 13 Analysis of scale effects for the pillar models A–D indicated in Fig. 11. **a** Simulated axial stress–axial strain response, **b** variation of deformation modulus (E_m) with axial strain, **c** fracture extension and coalescence for models B and C and **d** difference between maximum and minimum E_m normalised to model D

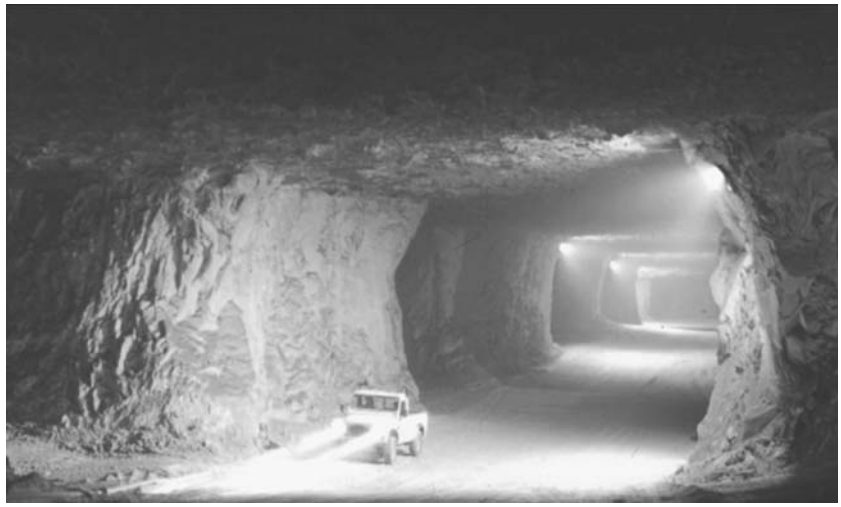

Fig. 14 View of Middleton Mine (after Pine et al. 2006)

wayboards (seams) of volcanic origin up to 0.5 m thick. The current study considers a number of different orthogonal cross sections through a FracMan model representing mapped jointed pillars at Middleton mine. The sections are then used to examine pillars of 2.8, 7 and 14 m wide × 7 m high (Fig. 15). The estimated range of areal fracture intensity P_{21} for Middleton mine is 1.8–2.6 (P_{21} is the ratio of total fracture length to area). The influence of fracture intensity with respect to the simulated pillar strength and failure mechanisms are investigated by additionally including models assuming a varied P_{21} value. The areal fracture intensity is reduced or increased by, respectively, deleting or inserting selected fractures in the original model. In order to minimise the user's intervention, a randomly generated number is used to identify the fractures to be deleted and the location (coordinates) of additional fractures.

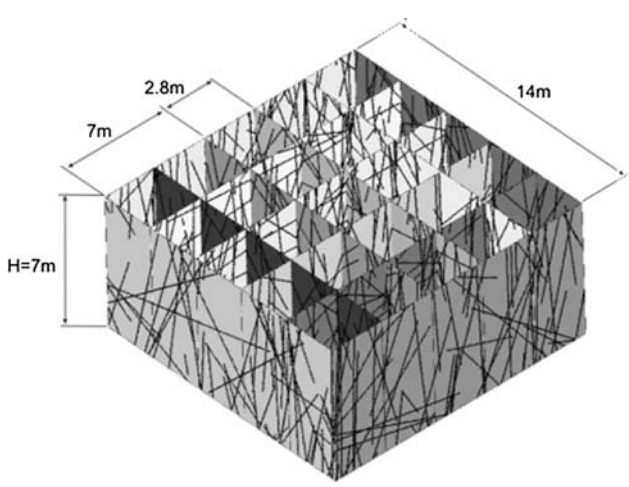

Fig. 15 Middleton mine FracMan pillar model showing the typical sampling planes used to define the 2D fracture traces models for ELFEN (after Elmo 2006)

Table 5 presents typical key input parameter values for the ELFEN geomechanics modelling. These values were derived from a combination of laboratory measurements on the Middleton limestone and values for similar limestones from the literature (e.g. Bearman 1991). For the Mohr–Coulomb intact rock constitutive criterion, values of cohesion c and internal angle of friction ϕ are also required. These were determined from the value for σ_{ci} of 48 MPa and Hoek–Brown parameters of $s = 1$ and $m_i = 9$ (typical for limestone), over a limited range of confining stress, using the program RocLab (Rocscience 2007; Hoek et al. 2002).

5.1 Modelling Results

As discussed in Sect. 4.1, the behaviour under uniaxial loading of relatively slender pillars may be significantly controlled by natural jointing conditions, and furthermore slender pillars may be expected to display critical aspects of the failure process in the early stages of the simulation. The Middleton mine case study has therefore included many simulations of pillars with a width of 2.8 m and a W:H ratio of 0.4. Different combinations of fracture intensity have been considered in the modelled pillars, including values outside the estimated P_{21} range of 1.8–2.6.

The analysis indicates that the overall influence of the natural fractures diminishes with increasing fracture intensity, as discussed by Diederichs et al. (2002) (Fig. 16). For $P_{21} < 0.2$ the pillars behave as an almost massive rock mass. For $P_{21} > 2.9$, due to the relatively higher degree of fracturing, the pillars response is almost isotropic. Conversely, for P_{21} in the range of 0.2–2.9 the strength of the simulated slender pillars is highly variable and clearly dependent on the inclination, spacing and persistence of the discontinuities. The analysis is

Table 5 Middleton mine case study, assumed modelling rock mass properties

Property (rock mass)	Unit	Value	Property (joints)	Unit	Value
Tensile strength, σ_t	MPa	3.8	Fracture cohesion, c_f	MPa	0.225
Fracture energy, G_f	J m^{-2}	19	Fracture friction, ϕ_f	°	35
Young's modulus, E	MPa	27,000	Normal penalty, P_n	GPa m^{-1}	27
Poisson's ratio, ν		0.3	Tangential penalty, P_t	GPa m^{-1}	2.7
Internal cohesion, c_i	MPa	9			
Internal friction, ϕ_i	°	45			

Joint cohesion and friction derived based on shear box tests

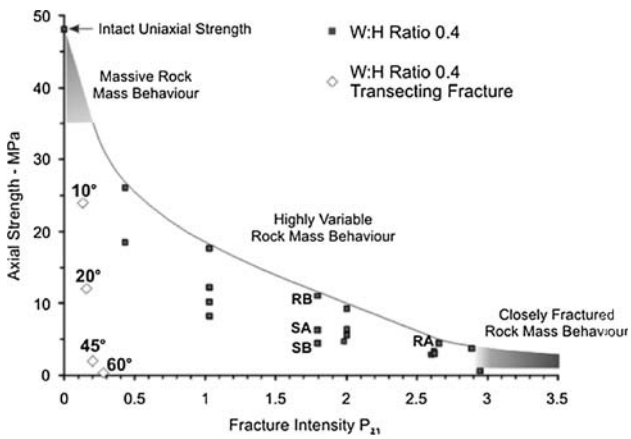

Fig. 16 Variation of the simulated pillar strength with fracture intensity for different prefractured 2.8 m × 7 m pillar models. The figure also includes the modelling results for a pillar of similar size and containing a single intersecting fracture (10°, 20°, 45° and 60° joint inclination). Models SA–SB and RA–RB refer to Figs. 17 and 23, respectively

complemented by including modelling results for a pillar of similar size containing a single intersecting fracture. The observed variability of strength estimates for equivalent fracture intensity P_{21} is associated with the jointing character of the rock mass and relates also to the importance of considering failure through intact rock bridges; for instance, Fig. 17 shows the mechanical response and fracture evolution at peak stress for two models with equal P_{21} but different P_{20} (number of fractures per unit area). In comparison with model SB, in model SA selected fractures have been split at their mid-point by introducing a 0.2-m-long intact rock bridge. In order to compensate for the reduced length, the fractures have been extended at their opposite edges by a factor equal to the newly introduced rock bridge (0.1 m each side). The modelling results illustrate the importance of fracture persistence in moderately jointed rock masses. The modelled rock bridges are clearly responsible for the increased self-supporting capacity of the rock mass. The results appear to agree with observations by Diederichs (2003), who stated that, even when they occupy only a very small percentage of the discontinuity-coplanar area, intact rock bridges could provide internal or self-supporting load-carrying capacity equivalent to conventional underground support systems. The strength simulated in model SB is 30% lower than model SA, and failure primarily occurs as a combination of sliding and rotation of blocks. A relative softer post-peak response is observed for model SB compared with model SA, which behaves in a more brittle manner.

Figure 18 shows that for the pillars mapped at the Middleton mine the degree of variability of pillar strength is clearly a function of pillar shape. An anisotropy index is

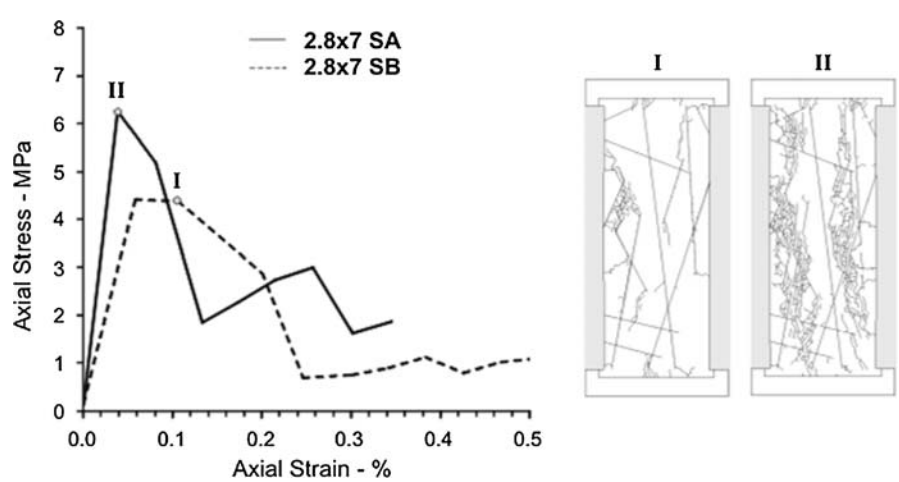

Fig. 17 Stress–strain response and fracturing evolution at peak stress models for models SA and SB, respectively. The two models differs by the introduction in model SA of 0.2 m rock bridges at mid-point of the predefined fractures

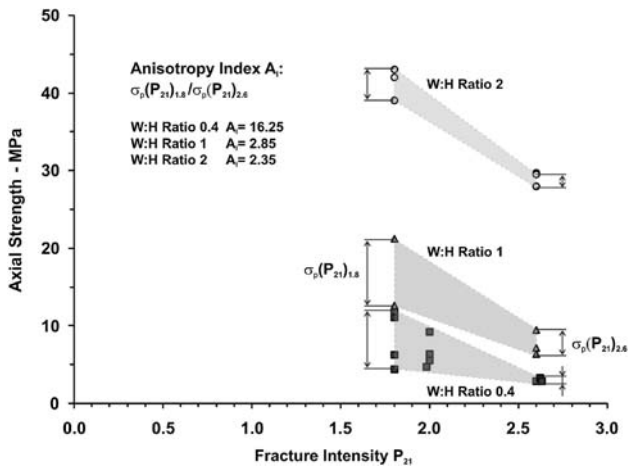

Fig. 18 Analysis of shape effects. Results for Middleton mine (UK) and modelled rock pillars with height of 7 m and width of 2.8, 7 and 14 m, respectively (modified from Elmo 2006)

derived (A_I), expressed as the ratio of the simulated pillar strength (range) for $P_{21} = 1.8$ to the simulated strength for $P_{21} = 2.6$. The decreasing A_I value with increasing pillar width suggests that, for relatively wider pillars, the response to loading may be investigated using a continuum approach with the assumption of isotropic rock mass behaviour. However, for cases including intersecting structural features or one of the discontinuity sets being significantly weaker than the others, the stability of the pillar may be better analysed using approaches that can truly capture failure mechanisms involving the sliding and/or rotation of blocks.

Figure 19a presents profiles of the vertical stress distribution across the mid-height for one of the 7 m × 7 m pillar models (fracture intensity $P_{21} = 2.6$) whilst the complete stress–strain response is given in Fig. 19b. The asymmetric nature of the load development, through the sequence of loading stages (I–III) is evident. The longer pre-existing fractures appear to channel stress concentrations. The process can be better observed referring to Fig. 20, which includes both the fracturing evolution and the maximum to minimum principal stress ratio plots for the same loading stages. Similar results are shown in Fig. 21 for a selected 14 m × 7 m pillar model (fracture intensity $P_{21} = 2.6$). The analysis clearly captures the different failure mechanisms taking place in the pillar sidewalls. Limited new fracturing and lateral spalling occur in the early stages of the simulations, followed by additional fracturing of the intact core as the loading of the pillar is increased. Lateral spalling may include the displacement of large blocks, but overall does not compromise the effective bearing capacity of the pillars, the increased confinement being responsible for the higher measured pillar strengths and the lower deformability. The development of pillar hourglassing, as the loading is increased, is apparent when observing the maximum/minimum principal stress vector plots.

Figure 22 compares the results of several of the simulations described above together with published empirical results for a variety of pillar types. All are presented as average capacity (stress) normalised to the intact σ_{ci} values against the pillar W:H ratio. The modelled behaviour indicates a rapidly increasing average strength with increase in W:H ratio. This type of behaviour is more commonly predicted for squat or barrier-type pillars at higher W:H ratios (Madden 1991), but is also seen at similar lower W:H ratios with Hoek–Brown brittle fracture modelling (Martin and Maybee 2000).

The practice of developing slender pillars is typically pursued in order to maximise extraction ratio, although this was not the case for the Middleton mine. The current analysis indicates that the level of uncertainty associated with the natural variability of the jointing conditions is much greater for slender pillars. Wiles (2006) has proposed the use of a coefficient of variation, C_p, to quantify the uncertainties associated with numerical modelling predictions, including uncertainties relative to rock mass strength, mining stress and modelling procedures. More significantly, the same author has recognised that different values of factor of safety are required to give the same probability of failure depending on the value of C_p. The higher level of uncertainty associated with the geological structure within a jointed slender pillar could be represented by a higher C_p value. Similarly, the anisotropy index introduced in Fig. 18 suggests that rock mass strength equations developed from

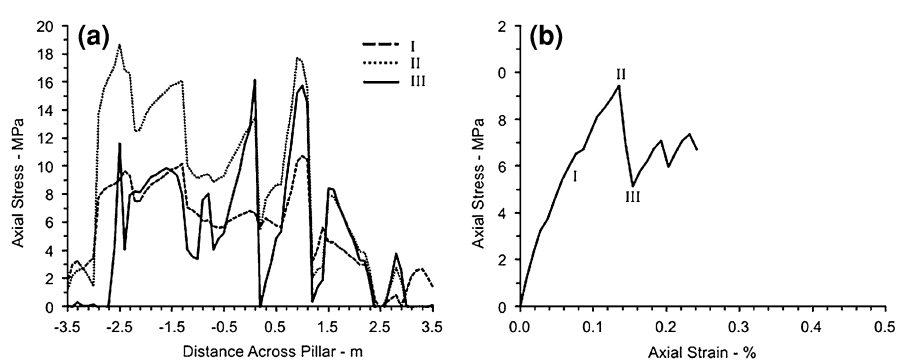

Fig. 19 **a** Axial stress profile at loading stages I–III for one of the 7 m × 7 m pillar models and **b** complete stress–strain response

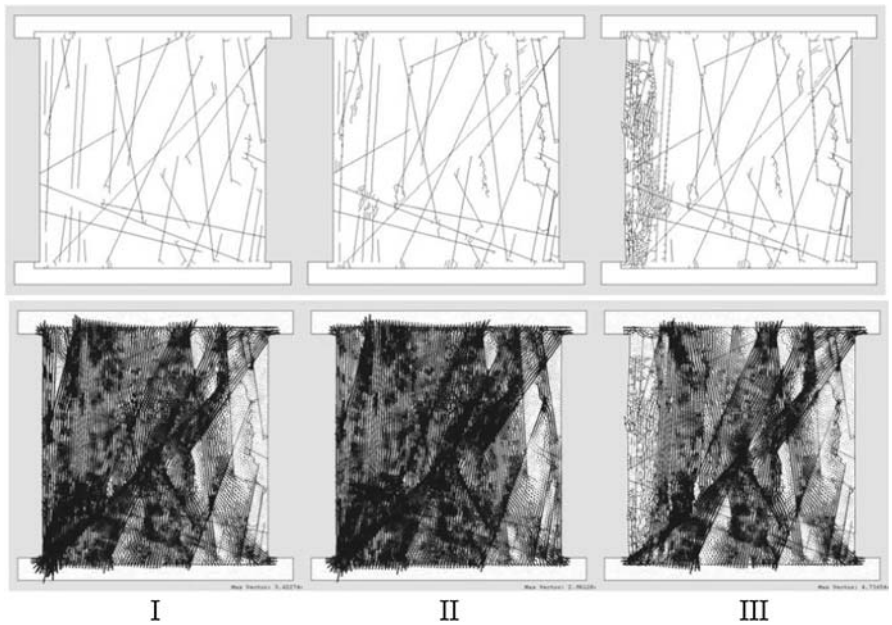

Fig. 20 Fracturing evolution and principal stress vector plots for the same loading stages indicated in Fig. 19

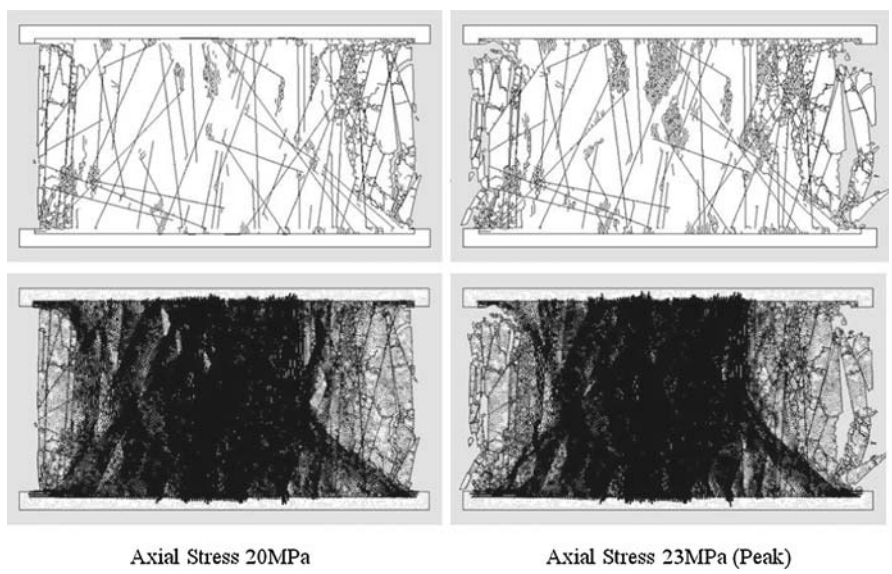

Fig. 21 Fracturing evolution and principal stress vector plots for a 14 m × 7 m pillar model, showing the development of hourglassing

empirical studies may fail to predict significantly the different strength estimates associated with a different combination of fracture intensity and jointing conditions. A major implication is that a higher factor of safety would be required when designing slender pillars to account for this variability, as also discussed by Esterhuizen (2006).

6 Towards the Development of Synthetic Rock Mass Properties

Rock mass characterisation systems such as the rock mass rating system (RMR; Bieniawski 1989), Q-index (Barton et al. 1974) and the geological strength index (GSI; Hoek et al. 1992, 1995) are useful tools which serve the purpose of (1) identifying significant parameters influencing rock mass behaviour, (2) deriving quantitative data for engineering design and (3) providing a quantitative measure to compare geological conditions at different sites. The GSI index has the advantage of being related to the Hoek–Brown failure criterion for rock masses, which is widely accepted in geotechnical and rock engineering applications. Establishing representative rock mass properties has long been recognised as one of the main challenges in rock mechanics. Rock mass classification systems such as the RMR, the Q-index or the coupled GSI/Hoek–Brown approach are traditionally used to derive properties for numerical analysis of rock engineering problems. Recently, 2D and 3D DEM techniques have been applied to the development of so-called synthetic rock mass properties

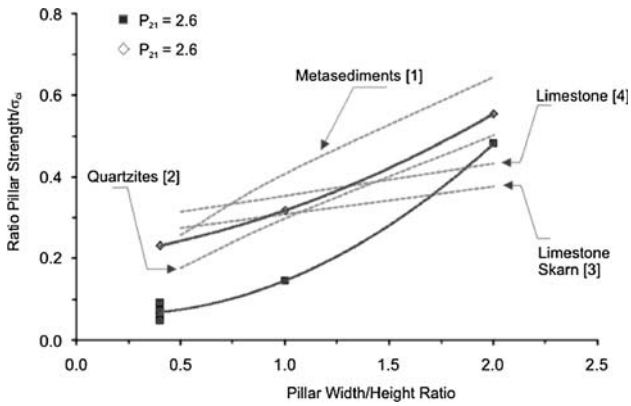

Fig. 22 Comparison between the results of several simulations described in the text ($P_{21} = 1.8$ and 2.6, respectively) and empirical results for a variety of pillar types. All are presented as average capacity (stress) normalised to the intact σ_{ci} values against the pillar W:H ratio. *[1]* Von Kimmelmann et al. (1984), *[2]* Hedley and Grant (1972), *[3]* Sjoberg (1992) and *[4]* Krauland and Soder (1987)

(e.g. Pierce et al. 2007), which combine the effects of the intact and fractured portions of the rock mass into a unique set of equivalent continuum properties. This approach allows engineers to model equivalent Mohr–Coulomb or Hoek–Brown strength envelopes, including anisotropic effects, by running suitable biaxial (in 2D) and triaxial (in 3D) test models of fractured rock masses. The test results can then be incorporated into a continuum finite element or finite difference model. The objective is to provide an improved link between mapped fracture systems and rock mass strength in comparison with the current practice of using empirical rock mass classifications alone.

By considering the effects of a lateral confinement, representing the horizontal stress component σ_3, the current analysis is extended to show the potential application of a coupled FEM/DEM-DFN approach in terms of providing estimates of rock mass properties. Models with σ_3 equal to 1, 2 and 4 MPa are presented (in addition to the unconfined case). Figure 23a and b shows a comparison between the RocLab-GSI curves (Rocscience 2007; Hoek et al. 2002) and the simulated σ_1–σ_3 response for 2.8 m × 7 m Middleton pillars with a fracture intensity P_{21} of 1.8 and 2.6, respectively. The RocLab-GSI curves are determined assuming $m_i = 12$ (typical of limestone), $\sigma_{ci} = 48$ and GSI values in the range of 70–80 and 40–50, respectively. These results demonstrate that it is possible to use a coupled DFN-fracture mechanics approach as a reliable measure of rock mass strength. Indeed, the mechanical response of a fractured rock mass can be highly variable and, depending on the problem scale, may be too small to account for persistence and termination effects of natural discontinuities in a fully "averaged" manner (Sect. 4). Anisotropic effects can be induced in a simulated fractured rock mass simply by varying the angle between the applied major principal stress and the direction of the predefined fractures. For a highly anisotropic rock mass (Fig. 24), the modelled strength response corresponds to a major reduction in the "equivalent" GSI rating. However, the resulting synthetic response cannot be considered as truly representative of the rock mass behaviour, which rather reflects the predominant role of the predefined fracture network and the occurrence of structurally controlled failure.

Similarly, the modelling results (Figs. 16 and 18) indicate that the mechanical response of slender pillars (W:H ratio of 0.4) can be highly variable. The models RA and RB represent a form of upper-bound response and are assumed to illustrate noncritical jointing conditions. In principle, for these slender pillars different GSI estimates could correspond to similar P_{21} values. These remarks imply that the reliability of a fracture intensity parameter (e.g. P_{21}) as a suitable indicator of the structural character of the rock mass will necessarily be dependent on the size of the problem under consideration. These results contribute to reaffirm important aspects of modelling rock mass behaviour, including:

- An accurate geological model is required for any synthetic rock mass model to be considered realistic.
- The scale of the synthetic rock mass tests must be sufficient to capture the REV for local jointing conditions and, in order to accommodate structural anisotropy, should be repeated to allow for different orientations of σ_1 and σ_3 relative to the joint orientations.
- The proposed ELFEN-DFN synthetic rock mass approach for continuum analysis would be more

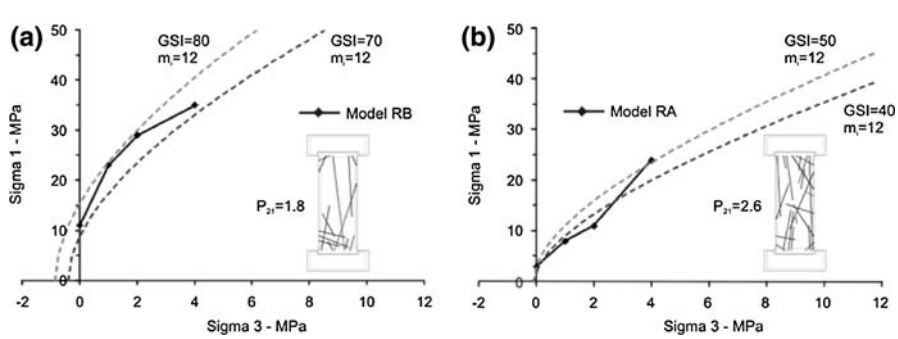

Fig. 23 Comparison between the ELFEN modelled response and the RocLab-GSI approach for the pillar models RB (**a**) and RA (**b**)

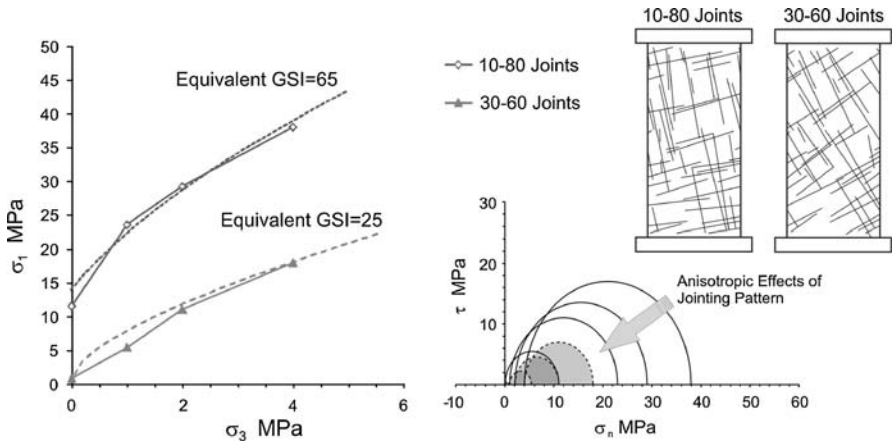

Fig. 24 Simulated anisotropic effects induced in a fractured rock mass by varying the angle between the applied principal stress direction and the inclination of the predefined fractures; 4 m × 8 m pillar models, intact rock material parameters are given in Table 2

realistic when undertaken in 3D. Subsequently, for large-scale modelling of rock mass behaviour, the presence, orientation and continuity of any large singular features (e.g. faults) could be included specifically in the continuum analysis.

Notwithstanding its preliminary nature, the current analysis has major implications for pillar design. The synthetic approach would allow engineers to simulate the rock mass response to loading fully accounting for existing jointing conditions, and failure criteria may be developed that reflect specific mining conditions. It is suggested that intact rock behaviour, joint surface conditions, fracture intensity, shape effects and isotropic/anisotropic loading conditions may eventually be combined within a single formulation characterising rock mass strength.

7 Summary and Conclusions

The understanding of progressive failure behaviour is important for the design of pillars. This paper has investigated the use of the hybrid FEM/DEM code ELFEN in studying the failure modes of jointed pillars. The proposed numerical approach allows the simulation of crack growth, accumulation and coalescence, enabling investigation of the interaction between newly generated and pre-existing fractures and capturing the subsequent displacement and/or rotation of independent blocks. The strength of the approach is that the anisotropic, inhomogeneous spatial distribution and influence of the jointing are fully accounted for and the resulting deformation and failure mechanisms are considered to be more realistically simulated.

A fracture network system for the Middleton mine has been generated using the code FracMan and imported into ELFEN via a specific interface, which has allowed the definition of 2D prefractured models of pillars. The analysis has considered pillars with W:H ratios of 1:2.5, 1:1 and 2:1, respectively. Although, there is no direct evidence from actual field-scale pillar failures at the Middleton mine the overall simulated progression of failure and associated stress distributions appear to be realistic. The analysis has demonstrated that the strength of slender pillars is predominantly influenced by naturally occurring fractures, and that slender pillars are particularly highly sensitive to the presence of inclined discontinuities. An anisotropy index has been introduced to characterise the highly variable rock mass strength estimated for the simulated slender pillars; this index is assumed to be a function of several factors, including fracture intensity, jointing conditions and associated occurrence of intact rock bridges. The higher level of uncertainty associated with jointed slender pillars could be represented by a higher value of the anisotropy index A_I or the coefficient of predictability C_p (Wiles 2006), which would correspond, under similar conditions, to a required higher factor of safety.

The ELFEN results demonstrate that it is possible to use mapped fracture intensity values as an indicator of the structural character of the rock mass. Additionally, the results are interpreted as indirectly confirming the coupled GSI-RocLab approach as a reliable measure of rock mass strength. It is noted that this verification is the result of numerical analysis of simulated rock pillars and is not derived from direct observations and empirical approaches. Further work is required using an observational method approach as suggested by Wiles (2006) to extend the current analysis. In this context, slender rock pillars represent a situation where an observable stress-induced response occurs repeatedly; therefore they are well suited to the application of an observational approach to design.

It is recognised that model uncertainty increases with the scale of the problem under consideration. When using numerical codes which are capable of simulating failure of the intact rock material, an important question arises as to whether the modelling of brittle fracture is undertaken at an appropriate scale. The answer to this question has certainly

far reaching connotations (Stead et al. 2007). To date the ELFEN modelling of fractured rock pillar has been limited to 2D analysis. However, 2D modelling has provided an important foundation on which to base ongoing 3D modelling of fractured pillars. Further 3D simulations are required in order to examine mean block size distribution and fragmentation changes during pillar failure.

Acknowledgements The authors would like to acknowledge financial support provided through NSERC Discovery and FRBC Endowment funds provided to the second author. Support and documentation relating to FracMan, provided by Golder Associates (Dr. Steve Rogers), are greatly appreciated. Support and material relating to ELFEN was provided by Rockfield Software. Mapping at Middleton mine was carried out as part of a project funded by the Engineering and Physical Sciences Research Council of the UK. The main component of the ELFEN modelling for Middleton mine was undertaken by the corresponding author as part of his Ph.D. thesis at the Camborne School of Mines (University of Exeter, UK) under the supervision of Prof. R.J. Pine and Dr. J.S. Coggan.

References

Barton N, Lien R, Lunde J (1974) Engineering classification of rock masses for the design of rock support. Rock Mech 6:189–236

Bearman RA (1991) The application of rock-mechanics parameters to the prediction of crusher performance. Ph.D. thesis, Camborne School of Mines, Penryn, UK

Bieniawski ZT (1989) Engineering rock mass classification. Wiley, New York, p 251

Brady B, Brown ET (1993) Rock mechanics for underground mining, 2nd edn. Chapman and Hall, London, p 588

Cai M, Kaiser PK (2004) Numerical simulation of the Brazilian test and the tensile strength of anisotropic rocks and rocks with pre-existing cracks. In: Proceedings of the SINOROCK international symposium on rock mechanics: rock characterization, modelling and engineering design methods, 18–21 May, Three Gorges Project site, China. Paper 2B-03

Coggan JS, Stead D (2005) Numerical modelling of the effects of weak mudstone on tunnel roof behaviour. In: Proceedings of the 58th Canadian Geotechnical Conference. Saskatoon, Canada. Paper GS502, p 9

Dershowitz W, Lee G, Geier J, LaPointe PR (1998) FracMan: interactive discrete feature data analysis, geometric modelling and exploration simulation. User documentation. Golder Associates Inc., Seattle

Diederichs MS (2003) Rock fracture and collapse under low confinement conditions. Rock Mech Rock Eng 36:339–381

Diederichs MS, Coulson A, Falmagne V, Rizkalla M, Simser B (2002) Applications of rock damage limits to pillar analysis at Brunswick Mine. In: Hammah R, Bawden W, Curran J, Telesnicki M (eds) Mining and tunnelling innovation and opportunity. Proceedings of the 5th North American rock mechanics symposium and 17th Tunnelling Association of Canada conference, Toronto, University of Toronto Press, Toronto

Eberhardt E, Stead D, Coggan JS (2004) Numerical analysis of initiation and progressive failure in natural rock slopes-the 1991 Randa rockslide. Int J Rock Mech Min Sci 41:69–87

Elmo D (2006) Evaluation of a hybrid FEM/DEM approach for determination of rock mass strength using a combination of discontinuity mapping and fracture mechanics modelling, with particular emphasis on modelling of jointed pillars. Ph.D. thesis. Camborne School of Mines, University of Exeter, UK

Elmo D, Coggan JS, Pine RJ (2005) Characterisation of rock mass strength by combination of field mapping and numerical modelling. In: Proceedings of the 40th US rock mechanics symposium, Anchorage, Alaska

Elmo D, Vyazmensky A, Stead D, Rance J (2008) Numerical analysis of pit wall deformation induced by block-caving mining: a combined FEM/DEM-DFN synthetic rock mass approach. In: Proceedings of the 5th conference and exhibition on mass mining, Lulea, Sweden, June 2008, p 10

Esterhuizen GS (2006) An evaluation of the strength of slender pillars. SME annual meeting and exhibit, March 27–29, St. Louis, Missouri, preprint 06-003. Society for Mining, Metallurgy, and Exploration, Inc., Littleton

Fang Z, Harrison JP (2002) Numerical analysis of progressive fracture and associated behaviour of mine pillars by use of a local degradation model. Trans Inst Min Metall 111:A59–A72

Golder Associates (2007) FracMan Technology Group, Golder Associates. http://www.fracman.golder.com

Hedley DGF, Grant F (1972) Stope-and-pillar design for the Elliot lake uranium mines. Bull Can Inst Min Metall 65:37–44

Hoek E, Brown ET (1980) Underground excavations in rock. Institution of Mining and Metallurgy, London, p 527

Hoek ET, Kaiser PK, Bawden WF (1995) Support of underground excavations in hard rock. A.A. Balkena, Rotterdam, p 215

Hoek ET, Carranza Torres C, Corkum B (2002) Hoek–Brown failure criterion-2002 edition. In: RocLab user's manual. Rocscience. http://www.rocscience.com

Karami A, Stead D (2008) Asperity degradation and damage in the direct shear test: a hybrid DEM/FEM approach. Rock Mech Rock Eng 41:229–266

Klerck PA (2000) The finite element modelling of discrete fracture in quasi-brittle materials. Ph.D. thesis, University of Wales, Swansea

Krauland N, Soder PE (1987) Determining pillar strength from pillar failure observations. Eng Min J 8:34–40

Madden BJ (1991) A re-assessment of coal-pillar design. J S Afr Inst Min Metallurgy 90(1):27–37

Martin CD, Maybee WG (2000) The strength of hard-rock pillars. Int J Rock Mech Min Sci 37:1239–1246

Munjiza A (2004) The combined finite-discrete element method. Wiley, Chichester, p 348

Nordlund E, Radberg G, Jing L (1995) Determination of failure modes in jointed pillars by numerical modelling. In: Fractured and jointed rock masses. Balkema, Rotterdam, pp 345–350

Owen DRJ, Feng YT, de Souza Neto EA, Cottrell MG, Wang F, Andrade Pires FM, Yu J (2004) The modelling of multi-fracturing solids and particulate media. Int J Numer Methods Eng 60(1):317–339

Pierce M, Cundall P, Potyondy D, Mas Ivars D (2007) A synthetic rock mass model for jointed rock. In: Proceedings of the 1st Canada–US rock mechanics symposium, vol 1. Vancouver, pp 341–349

Pine RJ, Harrison JP (2003) Rock mass properties for engineering design. Q J Eng Geol Hydrogeol 36:5–16

Pine RJ, Coggan JS, Flynn ZN, Elmo D (2006) The development of a new numerical modelling approach for naturally fractured rock masses. Rock Mech Rock Eng 39(5):395–419

Pine RJ, Owen DRJ, Coggan JS, Rance JM (2007) A new discrete modelling approach for rock masses. Geotechnique 57(9):757–766

Roberts DP, Lane WL, Yanske TR (1998) Pillar extraction at the Doe run Company, 1991–1998. AusIMM 1998-the mining cycle, pp 227–233

Roberts D, Tolfree D, McIntire H (2007) Using confinement as a means to estimate pillar strength in a room and pillar mine. In:

Proceedings of the 1st Canada–US rock mechanics symposium, vol 2. Vancouver, pp 1455–1462

Rockfield (2007) Rockfield Software Ltd. Technium, Kings Road, Prince of Wales Dock, Swansea, SA1 8PH, UK. http://www.rockfield.co.uk

Rocscience (2007) RocLab user's manual. http://www.rocscience.com

Singh M, Rao KS, Ramamurthy T (2002) Strength and deformational behaviour of a jointed rock mass. Rock Mech Rock Eng 35(1):45–64

Sjoberg J (1992) Failure modes and pillar behaviour in the Zinkgruvan mine. In: Proceedings of 33rd US rock mechanics symposium. Santa Fe. Balkema, Rotterdam, pp 491–500

Stead D, Coggan JS, Eberhardt E (2004) Realistic simulation of rock slope failure mechanisms: the need to incorporate principles of fracture mechanics. In: Proceedings of SINOROCK international symposium on rock mechanics: rock characterization, modelling and engineering design methods, 18–21 May, Three Gorges Project site, China. Paper 2B-17

Stead D, Coggan JS, Elmo D, Yan M (2007) Modelling brittle fracture in rock slopes: experience gained and lessons learned. In: Proceedings of international symposium. Rock slope stability in open pit mining and civil engineering. Perth, Australia

Stefanizzi S (2007) Numerical modelling of strain-driven fractures around tunnels in layered materials. Ph.D. thesis. University of Turin, Italy

Von Kimmelmann MR, Hyde B, Madgwick RJ (1984) The use of computer applications at BCL limited in planning pillar extraction and design of mining layouts. In: Proceedings of ISRM symposium design and performance of underground excavations. Geotechnical Society, London, pp 53–63

Vyazmensky A, Elmo D, Stead D, Rance J (2008) Numerical analysis of the influence of geological structures on development of surface subsidence associated with block caving mining. Proceedings of the 5th conference and exhibition on mass mining, Lulea, Sweden, June 2008, p 10

Wiles TD (2006) Reliability of numerical modelling predictions. J Rock Mech Min Sci 43:454–472

Yan M, Stead D, Sturzenegger M (2007) Step-path characterization in rock slopes: an integrated numerical modelling-digital imaging approach. In: Proceedings of 11th congress of the international society for rock mechanics. Lisbon, 9–13 July 2007, pp 693–696